# A computational paradigm for multiresolution topology optimization (MTOP)

**Tam H. Nguyen · Glaucio H. Paulino ·
Junho Song · Chau H. Le**

**Abstract** This paper presents a multiresolution topology optimization (MTOP) scheme to obtain high resolution designs with relatively low computational cost. We employ three distinct discretization levels for the topology optimization procedure: the *displacement mesh* (or finite element mesh) to perform the analysis, the *design variable mesh* to perform the optimization, and the *density mesh* (or density element mesh) to represent material distribution and compute the stiffness matrices. We employ a coarser discretization for finite elements and finer discretization for both density elements and design variables. A projection scheme is employed to compute the element densities from design variables and control the length scale of the material density. We demonstrate via various two- and three-dimensional numerical examples that the resolution of the design can be significantly improved without refining the finite element mesh.

**Keywords** Topology optimization · Density mesh ·
Design variable · Multiresolution · Finite element mesh ·
Projection scheme

T. H. Nguyen · G. H. Paulino (✉) · J. Song · C. H. Le
Department of Civil and Environmental Engineering,
University of Illinois, Urbana, IL 61801, USA
e-mail: paulino@illinois.edu, paulino@uiuc.edu

T. H. Nguyen
e-mail: tnguyen3@illinois.edu

J. Song
e-mail: junho@illinois.edu

C. H. Le
e-mail: chaule2@illinois.edu

## 1 Introduction

Topology optimization using the material distribution method has been well developed and applied to a variety of applications such as structural, mechanical and material systems (Bendsøe and Kikuchi 1988; Rozvany 2001). The material distribution method (Bendsøe 1989) rasterizes the domain by defining the topology via the density of pixels/voxels, and thus a large number of design variables are usually required for a well defined design, especially in three-dimensional (3D) applications. Several studies have been devoted to developing efficient procedures to solve large-scale topology optimization problems. Most of the efforts focus on the finite element analysis since it constitutes the dominant cost in topology optimization. For example, Borrvall and Petersson (2001) solved 3D realistic topology optimization designs with several hundreds of thousands of finite elements using parallel computing with domain decomposition. Wang et al. (2007) introduced fast iterative solvers to reduce the computational costs associated with the finite element analysis of 3D topology optimization problems. Amir et al. (2009) proposed an approximate reanalysis procedure for the topology optimization of continuum structures. According to this procedure, the finite element analysis is only performed at an interval of several iterations and approximate reanalyses are performed for other iterations to determine the displacement. The authors showed that this rough approximation is acceptable in topology optimization. Another approach consists of using adaptive mesh refinement (AMR) to reduce the number of finite elements (Stainko 2006; de Sturler et al. 2008). de Sturler et al. (2008) tailored the AMR method to represent void regions with fewer (coarser) elements and solid regions, especially in material surface regions, with more (finer) elements. In a topology optimization problem,

where shape, size and position of the void and solid regions are unknown, the AMR method allows the finite element mesh to be refined during the optimization process.

The abovementioned studies mainly focus on reducing computational cost of large-scale problems to obtain high resolution design. However, the mesh representation may also improve the resolution. The existing element-based and nodal-based approaches can be interpreted with a design variable mesh and a displacement mesh. In the element-based approach, a uniform density of each displacement element is considered a design variable. In contrast, the nodal-based approaches (Guest et al. 2004; Rahmatalla and Swan 2004; Matsui and Terada 2004) consider the densities at nodes as the design variables. The element densities are then obtained from nodal values using projection. Because the projection scheme provides control over the local gradient of material density, it imposes a minimum length scale feature and alleviates the checkerboard problem. Recently, Paulino and Le (2009) proposed another choice of nodal design variables to obtain high resolution design for quadrilateral elements. According to their study, the nodal design variables can be located at the midpoints of the four edges of the quadrilateral element. The authors showed that these locations of the design variables result in a higher resolution topology design without increasing mesh refinement. Also in the study by de Ruiter and van Keulen (2004), the decoupling of topology definition and the finite element mesh was introduced by using topology definition function. Additionally, wavelets for design variables have been applied to topology optimization in order to obtain high resolution design (Kim and Yoon 2000; Poulsen 2002a). Guest and Genet (2009) reduced the computational cost of topology optimization by using adaptive design variables while keeping the same finite element mesh.

In this paper, we propose a multiresolution topology optimization (MTOP) approach for handling large-scale problems with relatively low computational costs. Our proposed MTOP approach focuses on using the concept that the finite element mesh, density element mesh, and design variable mesh are distinct. In this study, the analysis is performed on a coarser finite element mesh, optimization is performed on a fine design variable mesh, and element densities are defined on a finer mesh. Therefore, the total computational cost is reduced compared to uniformly using fine meshes. Since topology is defined on the fine density element mesh, high resolution design is obtained. We can employ different density element/design variable meshes from coarse to fine, therefore, multiresolution designs can be obtained for the same finite element mesh.

This paper is structured as follows: Section 2 provides an overview of the topology optimization formulation; Section 3 describes the concept and implementation of the proposed MTOP approach; Section 4 presents two-

dimensional (2D) numerical examples, which explore conceptual aspects of the proposed approach; Section 5 shows 3D numerical examples, which illustrate the MTOP solution of relatively large problems; and Section 6 presents the conclusions.

## 2 Topology optimization formulation

In this section, the problem formulation of topology optimization is reviewed. The integration procedure of the stiffness matrix for the element-based approach and continuous approximation of material distribution (CAMD) approach (Matsui and Terada 2004), one of the nodal-based approaches, is also discussed.

### 2.1 Problem statement and formulation

In continuum structures, topology optimization aims to optimize the material densities which are considered design variables in a specific domain. In this study, minimum compliance is considered to maximize the stiffness of the structure while satisfying a volume constraint. Considering a reference domain $\Omega$ in $\mathbb{R}^2$ or $\mathbb{R}^3$, the optimization problem is defined as the problem of finding the choice of the stiffness tensor $E_{ijkl}(\mathbf{x})$ which is considered as variable over the domain. Let $U$ be the space of kinematically admissible displacement fields, $\mathbf{f}$ the body forces and $\mathbf{t}$ the tractions. The equilibrium equation is written in the weak, variational form (Bendsøe and Sigmund 2003). The energy bilinear form is as follows: $a(\mathbf{u}, \mathbf{v}) = \int_{\Omega} E_{ijkl}(\mathbf{x}) \varepsilon_{ij}(\mathbf{u}) \varepsilon_{kl}(\mathbf{v}) d\Omega$ with the linearized strains $\varepsilon_{ij}(\mathbf{u}) = \frac{1}{2} \left( \frac{\partial u_i}{\partial x_j} + \frac{\partial u_j}{\partial x_i} \right)$ and the load linear form given by $L(\mathbf{u}) = \int_{\Omega} \mathbf{f}\mathbf{u} d\Omega + \int_{\Gamma_T} \mathbf{t}\mathbf{u} ds$. The basic minimum compliance problem is expressed as

$$
\begin{aligned}
\min \quad & L(\mathbf{u}) \\
s.t.: \quad & a(\mathbf{u}, \mathbf{v}) = L(\mathbf{v}), \text{ for all } \mathbf{v} \in U \\
& \text{volume constraint}
\end{aligned}
\tag{1}
$$

The continuum problem statement (1) can be solved by using the finite element method. The basic problem statement is expressed in the discrete form as follows:

$$
\begin{aligned}
\min_{\rho} \quad & C(\rho, \mathbf{u}) = \mathbf{f}^{\mathrm{T}} \mathbf{u} \\
s.t.: \quad & \mathbf{K}(\rho) \mathbf{u} = \mathbf{f} \\
& V(\rho) = \int_{\Omega} \rho \, dV \leq V_s
\end{aligned}
\tag{2}
$$

where $\rho = \rho(\mathbf{x})$ is the density at position $\mathbf{x}$, $\mathbf{f}$ and $\mathbf{u}$ are the global load and displacement vectors, respectively, $\mathbf{K}$ is the global stiffness matrix, and $V_s$ is the prescribed volume. The desirable solution specifies if the density at any point in the domain is either 0 (void) or 1 (solid). However, it is impractical to solve the integer optimization problem. In a

relaxed problem, the density can have any value between 0 and 1. For example, in the popular model named solid isotropic material with penalization (SIMP; Rozvany et al. 1992; Bendsøe 1989; Bendsøe and Sigmund 1999), Young's modulus is parameterized using solid material density as follows

$$E(\mathbf{x}) = \rho(\mathbf{x})^p E^0 \tag{3}$$

where $E^0$ is the original Young's modulus of the material in the solid phase, corresponding to the density $\rho = 1$, and $p$ is the penalization parameter. To prevent singularity of the stiffness matrix, a small positive lower bound, e.g. $\rho_{\min} = 10^{-3}$, is placed on the density. Using the penalization parameter $p > 1$, the intermediate density approaches either 0 (void) or 1(solid).

$$0 < \rho_{\min} \leq \rho(\mathbf{x}) \leq 1 \tag{4}$$

In the element-based approach, the density of each element is represented by one value $\rho_e$ and the global stiffness matrix $\mathbf{K}$ in (2) is expressed as

$$\mathbf{K} = \sum_{e=1}^{N_{el}} \mathbf{K}_e(\rho_e) = \sum_{e=1}^{N_{el}} \int_{\Omega_e} \mathbf{B}^{\mathrm{T}} \mathbf{D}(\rho_e) \mathbf{B} d\Omega \tag{5}$$

where $\mathbf{K}_e(\rho_e)$ is the stiffness matrix of the element $e$, $\mathbf{B}$ is the strain-displacement matrix of shape function derivatives, and $\mathbf{D}(\rho_e)$ is the constitutive matrix which depends on the material density. For example, the formulation of the constitutive matrix for plane stress state is

$$\mathbf{D}(\mathbf{x}) = \frac{E(\mathbf{x})}{1 - \nu^2} \begin{bmatrix} 1 & \nu & 0 \\ \nu & 1 & 0 \\ 0 & 0 & (1 - \nu)/2 \end{bmatrix} \tag{6}$$

The solution of the gradient-based optimization problem in (2) requires the computation of sensitivities of the objective function and the constraint. In the element-based approach, element density $\rho_e$ is used as the design variable; therefore, these sensitivities can be obtained as follows

$$\begin{aligned} \frac{\partial C}{\partial \rho_e} &= -\mathbf{u}_e^{\mathrm{T}} \frac{\partial \mathbf{K}_e}{\partial \rho_e} \mathbf{u}_e = -p(\rho_e)^{p-1} \mathbf{u}_e^{\mathrm{T}} \mathbf{K}_e^0 \mathbf{u}_e \\ \frac{\partial V}{\partial \rho_e} &= \int_{\Omega_e} dV \end{aligned} \tag{7}$$

where $\mathbf{K}_e^0$ is the element stiffness matrix of the solid material.

## 2.2 Integration of the stiffness matrix

The stiffness matrix of each element in (5) is computed by integrating the stiffness integrand contribution over the displacement element domain. Numerical quadrature, such as Gaussian quadrature, is commonly reduced to the evaluation and summation of the stiffness integrand at specific Gauss points (Cook et al. 2002). The material density is also evaluated at the Gauss points during computation of the material property matrices.

In the element-based approach, the element density is represented by one design variable at the centroid of the element and the material densities of all the Gauss points are equal to the element density. In contrast, in the CAMD approach (Matsui and Terada 2004), the material densities at the Gauss points are computed from the nodal design variables and the stiffness matrices are evaluated at the Gauss points, i.e.

$$\begin{aligned} \mathbf{K}_e &= \int_{\Omega_e} \left( \sum_{i=1}^{N_{nod}} N_i(\mathbf{x}) \rho_i \right)^p \mathbf{B}^{\mathrm{T}} \mathbf{D}^0 \mathbf{B} d\Omega \\ &\simeq \sum_{g=1}^{N_n} \left( \sum_{i=1}^{N_{nod}} N_i(\mathbf{x}) \rho_i \right)^p \mathbf{K}_g^0 \end{aligned} \tag{8}$$

where $N_{\mathrm{nod}}$ is the number of nodes per element (e.g., $N_{\mathrm{nod}} = 4$ for Q4 and $N_{\mathrm{nod}} = 8$ for B8 element), $N_n$ is the number of Gauss points for integration, $N_i(.)$ is the $i$-th shape function, $i = 1, ..., N_{nod}$, $\mathbf{K}_g^0$ is the stiffness integrand at the Gauss point $g$, and $\mathbf{D}^0$ corresponds to the constitutive matrix of the solid material.

## 3 Multiresolution scheme in topology optimization

In this study, we call elements associated with the displacement mesh *displacement elements* and elements associated with the density mesh *density elements*. In light of the present work, existing element-based and nodal-based approaches can be interpreted with a design variable mesh and a displacement mesh. For example, in the element-based approach using Q4 element, a uniform density of each displacement element is considered a design variable so called Q4/U element. Figure 1 shows the element-based approach using Q4/U elements with the displacement mesh, the design variable mesh, and the superposed meshes. In this section, the concept and implementation of the MTOP approach will be discussed.

### 3.1 Multiresolution scheme and stiffness matrix integration

We employ three different meshes for the topology optimization problem: the *displacement mesh* to perform the analysis, the *design variable mesh* to perform the optimization, and the *density mesh* to represent material distribution and compute the stiffness matrices. Design variables are defined as the material densities at the center of the density
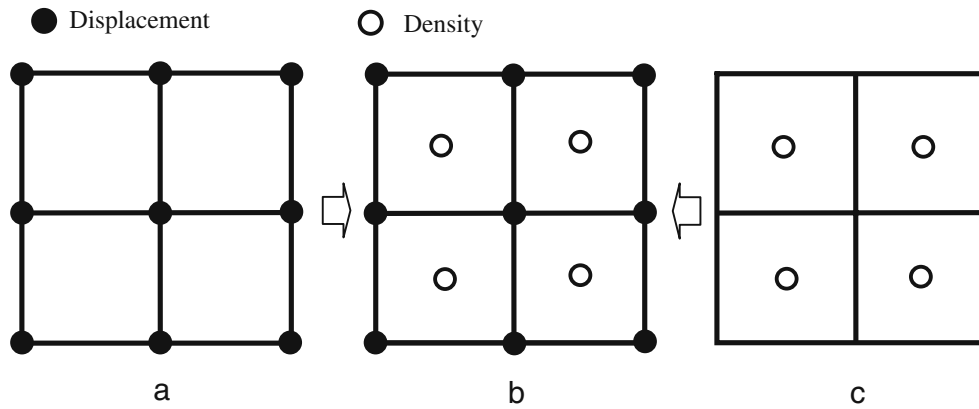
**Fig. 1** Q4/U elements: **a** Displacement mesh, **b** Superposed meshes, **c** Density mesh

elements. However, the design variable mesh and density mesh do not necessarily coincide. Design variables do not have physical meaning on their own. The design variable concept in this study is similar to the nodal design variable in the study by Guest et al. (2004). However, in their study, the design variables are associated with nodes of the finite element mesh, while in the MTOP scheme, the design variable mesh can be different from the finite element mesh. In our proposed scheme, the element densities are computed from the design variables by projection functions. The topology optimization problem definition in (2) is then rewritten accordingly:

$$
\begin{aligned}
\min_{\mathbf{d}} \ & C\left(\rho, \mathbf{u}\right) = \mathbf{f}^{\mathrm{T}}\mathbf{u} \\
s.t.: \ & \rho = f\left(\mathbf{d}\right) \\
& \mathbf{K}\left(\rho\right)\mathbf{u} = \mathbf{f} \\
& V\left(\rho\right) = \int_{\Omega}\rho dV \le V_{\mathrm{s}}
\end{aligned}
\tag{9}
$$

where $\mathbf{d}$ is the vector of design variables and $f(.)$ is the projection function.

To obtain high resolution design, we employ a finer density mesh than the displacement mesh so that each displacement element consists of a number of density elements (sub-elements). Within each density element, the material density is assumed to be uniform. Furthermore, a scheme to integrate the stiffness matrix, in which the displacement element consists of a number of different density elements, is introduced. For example, Fig. 2a shows a Q4 displacement element, Fig. 2b presents the multiple meshes, and Fig. 2c shows the density mesh with 25 density elements (also 25 design variables) per Q4 displacement. In the MTOP approach, we denote this element as Q4/n25 where "n25" indicates that the number of density elements "$n$" per Q4 is 25. The stiffness matrix is computed by evaluation of the stiffness integrand at the 25 integration points which are the centers of 25 density elements. The corresponding weight of the integrand is the area of the density element. The
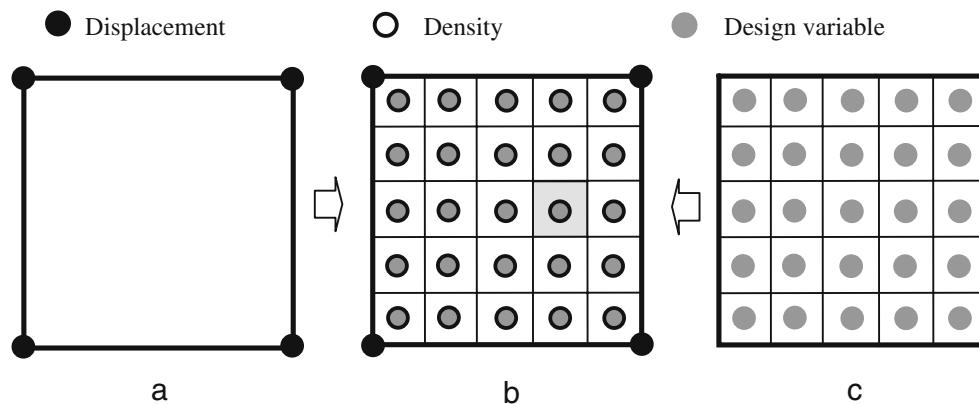


**Fig. 2** MTOP Q4/n25 element: **a** Displacement mesh, **b** Superposed meshes, **c** Design variable mesh

formulation for the stiffness matrix integration is expressed as follows

$$\mathbf{K}_e = \int_{\Omega e} \mathbf{B}^\mathrm{T}\mathbf{D}\mathbf{B}d\Omega \simeq \sum_{i=1}^{N_n} \left(\mathbf{B}^\mathrm{T}\mathbf{D}\mathbf{B}\right)\big|_i A_i \tag{10}$$

where $N_n$ is the number of integration points in the displacement element domain ($N_n$ is also equal to the number of density elements per displacement element), and $A_i$ is the contribution of density element $i$ to the integration ($A_i$ represents the area/volume of the density element for 2D/3D problems).

The SIMP interpolation model is employed to evaluate the stiffness matrix in (10) as follows

$$\mathbf{K}_e \simeq \sum_{i=1}^{N_n} (\rho_i)^p \left(\mathbf{B}^\mathrm{T}\mathbf{D}^0\mathbf{B}\right)\big|_i A_i = \sum_{i=1}^{N_n} (\rho_i)^p \mathbf{I}_i \tag{11}$$

where

$$\mathbf{I}_i = \left(\mathbf{B}^\mathrm{T}\mathbf{D}^0\mathbf{B}\right)\big|_i A_i. \tag{12}$$

The sensitivity of the compliance requires the computation of the sensitivity of the stiffness matrix with respect to the design variable, which can be calculated as

$$\frac{\partial \mathbf{K}_e}{\partial d_n} = \frac{\partial \mathbf{K}_e}{\partial \rho_i}\frac{\partial \rho_i}{\partial d_n} = \frac{\partial \left(\sum_{j=1}^{N_n} (\rho_j)^p \mathbf{I}_j\right)}{\partial \rho_i}\frac{\partial \rho_i}{\partial d_n} = (\rho_i)^{p-1} \mathbf{I}_i \frac{\partial \rho_i}{\partial d_n} \tag{13}$$

where $d_n$ and $\rho_i$ are the design variable and element density, respectively. The sensitivity analysis of the constraint in (9) is calculated similarly to (7) as follows

$$\frac{\partial V}{\partial d_n} = \frac{\partial V}{\partial \rho_i}\frac{\partial \rho_i}{\partial d_n}. \tag{14}$$

The sensitivity $\partial \rho_i / \partial d_n$ is presented in Section 3.3 on the projection method.

### 3.2 General element types and isoparametric elements

In addition to the quadrilateral element Q4/n25 discussed in Section 3.1, the MTOP approach can also be applied to other element types. For the 2D case, Fig. 3a shows a Wachspress hexagonal element (Talischi et al. 2009) with 24 density elements per displacement element (denoted by H6/n24), while Fig. 3b shows triangular element with 16 density elements per displacement element (T3/n16). For the 3D case, Fig. 3c shows 125 density elements per B8 element (B8/n125), while Fig. 3d shows the tetrahedral element with 64 density elements (TET4/n64).

The integration technique in (9) can also be used for isoparametric elements. For example, for a Q4 element with unit thickness in Fig. 4, the formulation to compute the stiffness matrix in the reference (parent) domain is as follows (Cook et al. 2002)

$$\mathbf{K}_e = \int_{\Omega e} \mathbf{B}^\mathrm{T}\mathbf{D}\mathbf{B}d\Omega = \int_{-1}^{1}\int_{-1}^{1} \mathbf{B}^\mathrm{T}\mathbf{D}\mathbf{B}J d\xi d\eta \tag{15}$$

where $(\xi, \eta)$ denote intrinsic coordinates in the interval $[-1,1]$, $J$ is the Jacobian, $\mathbf{B}$ is the strain-displacement matrix in the reference (parent) domain. The standard formulation of matrix $\mathbf{B}$ in the reference domain can be found in the literature (Cook et al. 2002). The integration of (15) in the reference domain can be computed as follows

$$\mathbf{K}_e = \int_{-1}^{1}\int_{-1}^{1} \mathbf{B}^\mathrm{T}\mathbf{D}\mathbf{B}J d\xi d\eta = \int_{\Omega 0} \mathbf{B}^\mathrm{T}\mathbf{D}\mathbf{B}d\Omega_0$$
$$\simeq \sum_{i=1}^{N_n} \left(\mathbf{B}^\mathrm{T}\mathbf{D}\mathbf{B}J\right)\big|_i A_i^0 \tag{16}$$

where $\Omega_0$ is the reference domain, $A_i^0$ is the area/volume of each density element $i$ in the reference domain as shown in Fig. 4.

### 3.3 Projection method: a minimum length scale approach

Without projection, the MTOP scheme above does not provide mesh independency, which might lead to numerical instability and checkerboard effects (Diaz and Sigmund 1995). Note that high resolution design has been the objective of various studies to alleviate the checkerboard patterns (Diaz and Sigmund 1995; Sigmund and Peterson 1998; Bourdin 2001; Bruns and Tortorelli 2001; Poulsen 2002a, b; Pomezanski et al. 2005). In this study, we use a variation of previously reported projection method (Guest et al. 2004; Almeida et al. 2009) to achieve minimum length scale and mesh independency. Our projection method uses design variables associated with design variable mesh to compute element densities which belong to density element mesh.
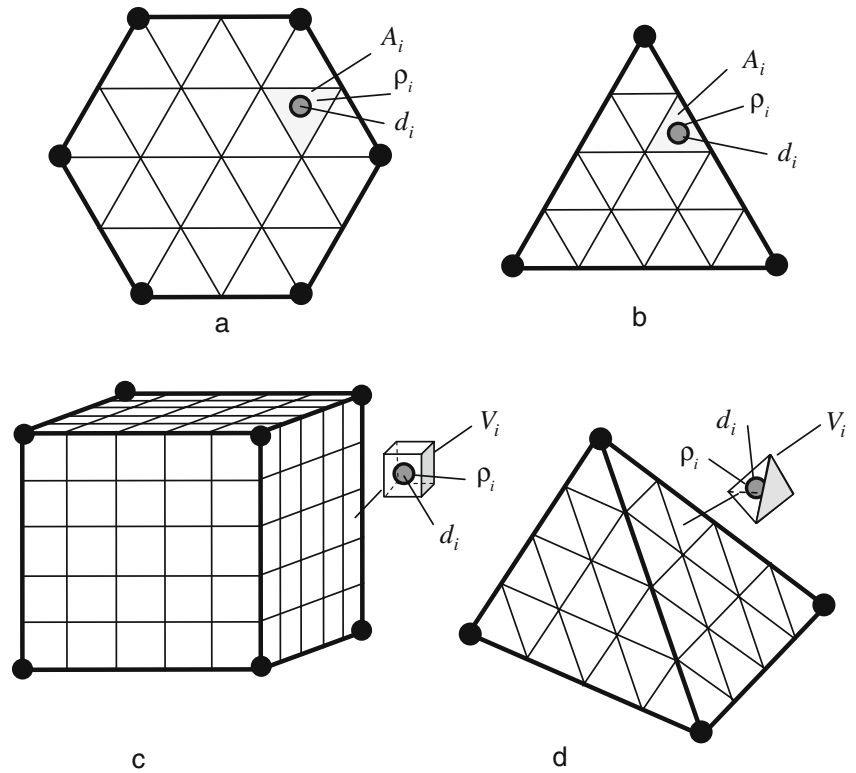
Here $d_n$ denotes the design variable associated with the design variable mesh, while $\rho_i$ represents the density of element $i$ associated with the density element mesh. Assume that the change of material density occurs over a minimum length of $r_{\min}$, as shown in Fig. 5. The element density $\rho_i$ is obtained from the design variables $d_n$ as follows

$$\rho_i = f(d_n) \tag{17}$$

where $f(.)$ is the projection function. For example, if a linear projection is employed, the uniform density of a density element is computed as the weighted average of the design variables in the neighborhood as follows

$$\rho_i = \frac{\sum_{n \in S_i} d_n w(\mathbf{x}_n - \mathbf{x}_i)}{\sum_{n \in S_i} w(\mathbf{x}_n - \mathbf{x}_i)} \tag{18}$$

**Fig. 4** Isoparametric element:
**a** Initial, **b** parent domain
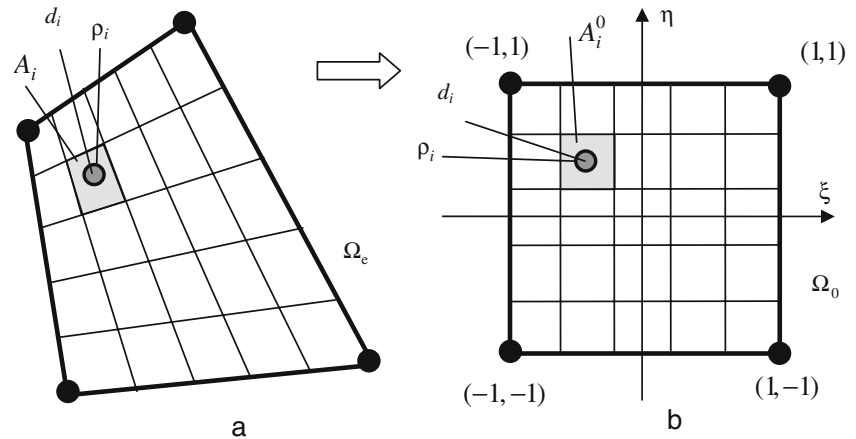
**Fig. 5** Projection function from the design variables to the density element
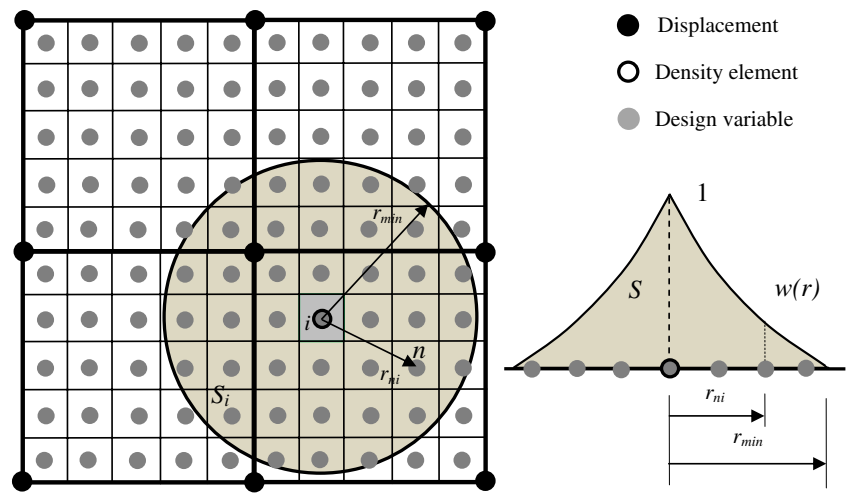


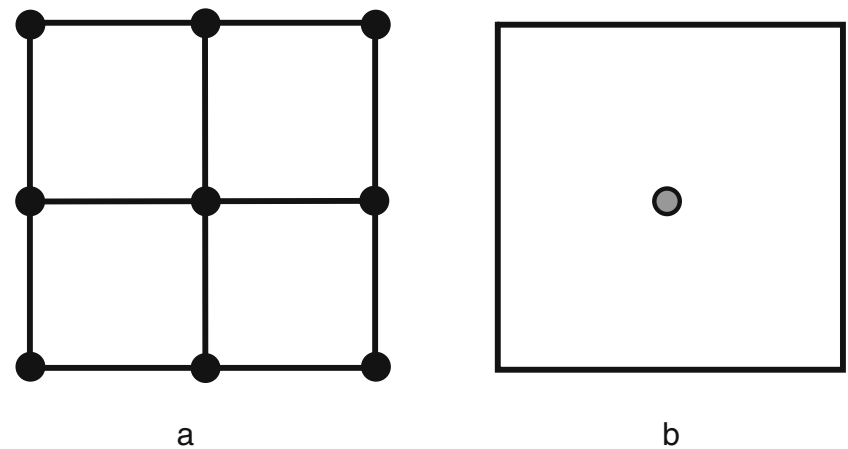**Fig. 6** Twenty five density elements of one displacement element
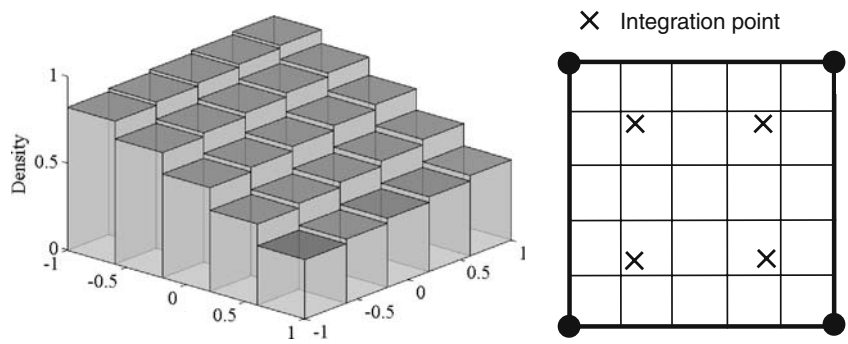


**Fig. 7** The MTOP approach for the super-element: **a** FE mesh, **b** Density/design variable mesh
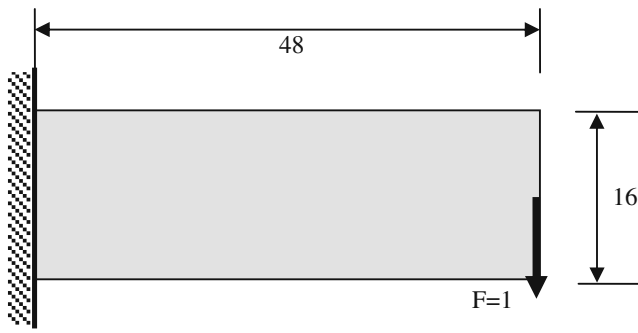


a

b

**Fig. 8** 2D cantilever beam



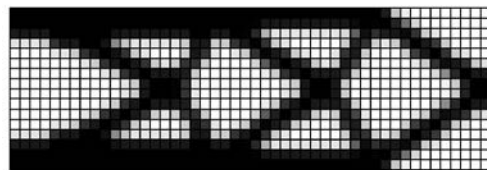**a** FE mesh size 240×80, element-based approach with Q4 elements (*C*=210.68)



**b** FE mesh size 48×16, MTOP Q4/n25 elements (*C*=208.23)

**Fig. 10** Topologies with the same resolutions (volfrac = 0.5, $p = 4$, $r_{\min} = 1.2$)

where $S_i$ is the sub-domain corresponding to density element $i$, $\mathbf{x}_n$ is the position of the point associated with design variable $d_n$. The corresponding weight function is defined as

$$w\left(\mathbf{x}_n - \mathbf{x}_i\right) = \begin{cases} \dfrac{r_{\min} - r_{ni}}{r_{\min}} & \text{if } r_{ni} \le r_{\min} \\ 0 & \text{otherwise} \end{cases} \quad (19)$$
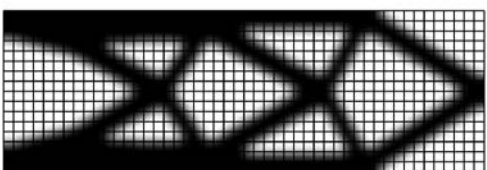
where $r_{ni}$ is the distance from the point associated with design variable $d_n$ to the centroid of density element $i$, and the physical radius $r_{\min}$ (see Fig. 5) is independent of the mesh.

The sensitivities of the element density in (18) with respect to design variables are derived as

$$\frac{\partial \rho_i}{\partial d_n} = \frac{w\left(\mathbf{x}_n - \mathbf{x}_i\right)}{\sum_{m \in S_i} w\left(\mathbf{x}_m - \mathbf{x}_i\right)}. \quad (20)$$

Using the projection function with a minimum length scale, the mesh independent solution is obtained.

### 3.4 Reduced number of integration points

During the optimization process, we may have regions with uniform material distribution, e.g. void region or solid regions. For these regions, the material distribution within elements is uniform, thus we can use regular integration for the element stiffness to further reduce the computational cost. For example, instead of using the 25 integration points,



**a** FE mesh size 48×16 (for both approaches)



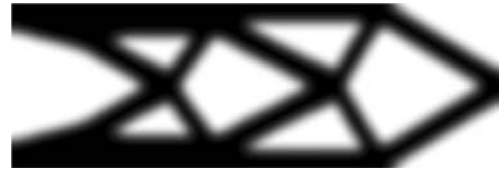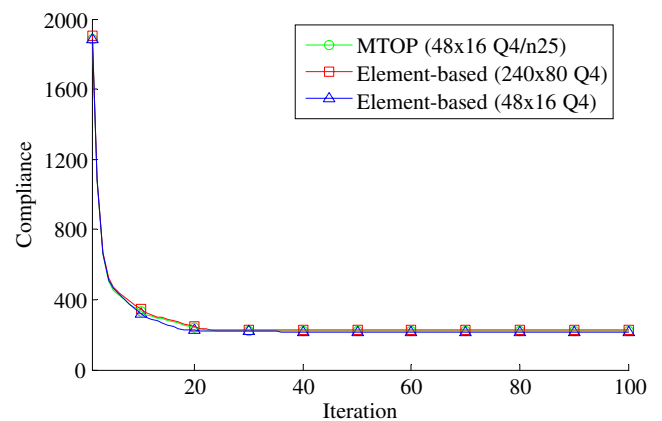**b** Element-based approach using Q4 elements (*C*=205.57)



**c** MTOP approach using Q4/n25 elements (*C*=208.23)

**Fig. 9** Topologies with the same FE mesh size $48 \times 16$ (volfrac = 0.5, $p = 4$, $r_{\min} = 1.2$)



**Fig. 11** Convergence history after 100 iterations

a MTOP 48×16 Q4/n4 elements



b MTOP 48×16 Q4/n9 elements
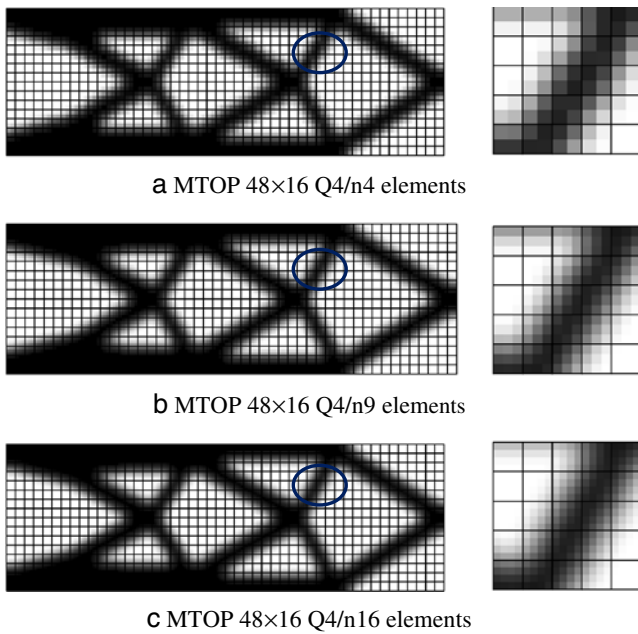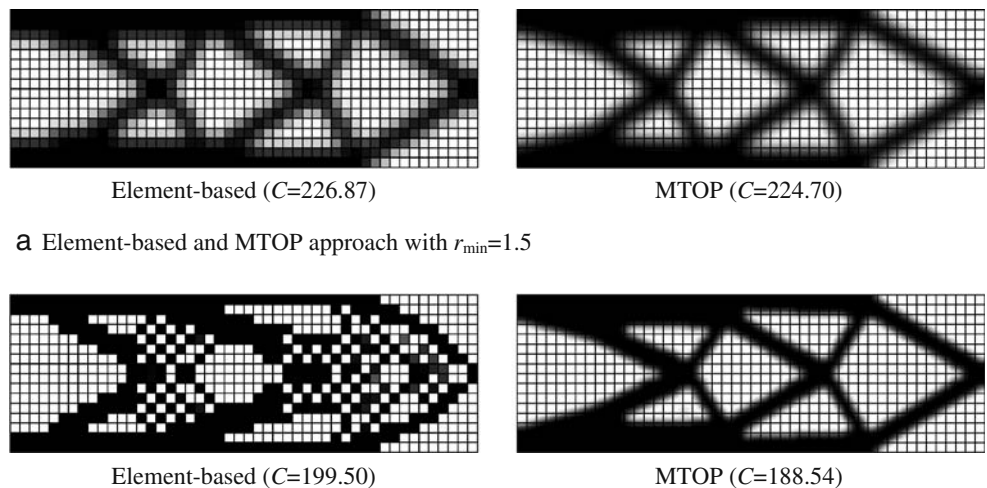


c MTOP 48×16 Q4/n16 elements

**Fig. 12** Multiresolution designs using MTOP (volfrac = 0.5, $p = 4$, $r_{min} = 1.2$)

we can perform the integration with fewer integration points such as 4 or 9 Gauss points. The locations of the Gauss points and the corresponding weights in the integration can be found in the literature (Cook et al. 2002). Figure 6 shows densities inside a typical displacement element with smooth change of density. Since the stiffness matrix integrand is evaluated at the Gauss points, the densities at these Gauss points are directly computed from the design variables using projection function.

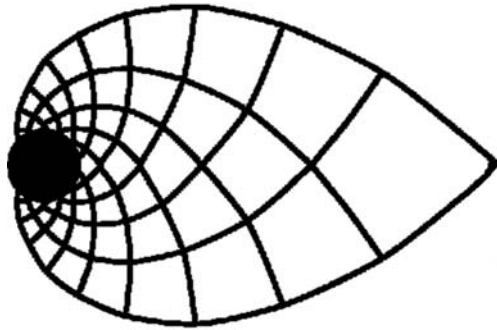### 3.5 Selection of displacement, density and design variable meshes

Our proposed MTOP approach generalizes some of the topology optimization methods such as element-based approach and super-element approach. For example, the element-based approach as shown in Fig. 1b can be obtained using an MTOP approach with Q4/n1 elements where each element density is represented by one design variable. In addition, the super-element approach (Paulino et al. 2008a, b) can be represented by our MTOP approach when special displacement, density element and design variable meshes, as shown in Fig. 7, are chosen. This mesh combination will result in the Q4 super-element which consists of several adjacent displacement elements having the same material density/design variable.

## 4 Two-dimensional numerical examples

This section illustrates the MTOP approach with 2D applications. A cantilever beam and the Michell truss benchmark examples are investigated. In all examples, SIMP model is employed to interpolate the stiffness tensor of the intermediate material density. The method of moving asymptotes (MMA; Svanberg 1987) is used as the optimizer. For simplicity, all the quantities are dimensionless. In addition, Young's modulus is chosen as 1 and Poison's ratio as 0.3 for all examples. Instead of using prescribed volume $V_s$ constraint in (1), we use volume fraction volfrac which is defined as the ratio of the prescribed volume $V_s$ and the total volume of the domain.

**Fig. 13** Element-based approach and MTOP with different minimum length scales



Element-based ($C$=226.87)



MTOP ($C$=224.70)

a Element-based and MTOP approach with $r_{min}$=1.5



Element-based ($C$=199.50)



MTOP ($C$=188.54)

b Element-based and MTOP approach with $r_{min}$=0.75

**a** Domain for Michell truss (mesh size 180×120)



**b** Analytical solution of Michell truss
(Taken from Sigmund 2000)



**c** MTOP optimal topology solution
(*volfrac* = 0.25, $p$ = 4, $r_{min}$ = 1.2)

**Fig. 14** Michell truss with a circular support

## 4.1 Cantilever beam

Figure 8 shows a 2D cantilever beam with length of 48, height of 16, and unit width. The beam is fixed at the left edge and a unit point load is applied downward at the midpoint of the right end. A volume fraction constraint volfrac is taken as 50%. The penalization $p$ is set equal to 4 and projection radius $r_{min}$ of 1.2 is used for calculations. The element-based approach Matlab code (Sigmund 2001; Bendsøe and Sigmund 2003), modified to utilize the MMA optimizer and the projection method instead of the sensitivity filter, was used as a reference for the results of the MTOP approach.

### 4.1.1 Two designs with the same displacement mesh size

The cantilever domain is discretized into mesh size of $48 \times 16$ using 768Q4 elements with unit-length as shown in Fig. 9a. The results obtained from element-based and MTOP approaches are shown in Fig. 9b and c, respectively. These figures show that for the same displacement mesh size, the topology obtained from MTOP has a much better resolution than that of the element-based approach.

### 4.1.2 Two designs with the same resolution

We investigate the displacement mesh requirements for the two abovementioned approaches to achieve topology designs with the same resolution. The element-based approach is performed on a displacement mesh of $240 \times 80$ as shown in Fig. 10a while the MTOP approach employs Q4/n25 elements with the coarse mesh size $48 \times 16$ as shown in Fig. 10b. These data show that the topology obtained from the MTOP approach on a coarse displacement mesh has the same resolution with that obtained from the element-based approach on a fine mesh.

### 4.1.3 Convergence history and computational cost

The convergence histories of the MTOP and the element-based approaches are compared in Fig. 11. During the optimization process, compliance convergence histories from the MTOP and element-based approaches for both coarse finite element mesh and fine finite element meshes are very similar. After 100 iterations, MTOP with a coarse mesh obtained a compliance of 208.23 while the element-based approach obtained 205.57 and 210.68 for a coarse mesh and a fine mesh, respectively.
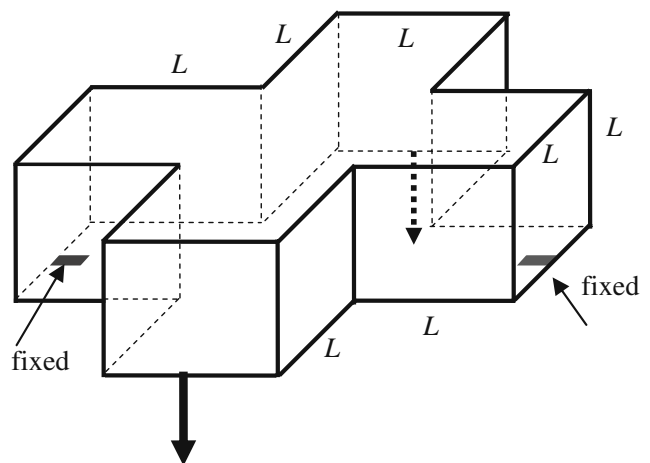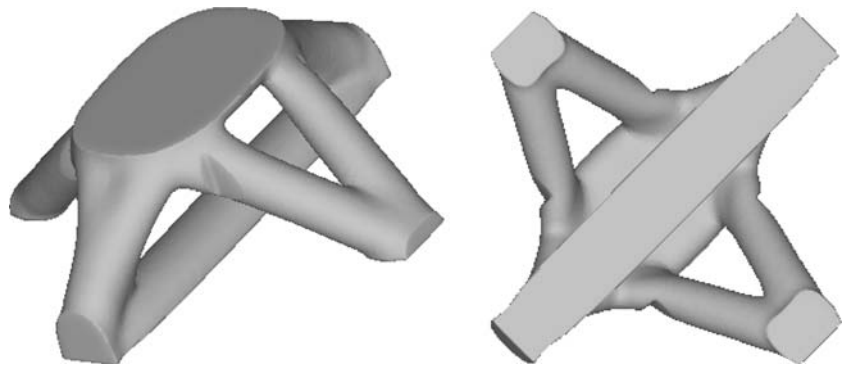


**Fig. 15** Geometry of the 3D cross-shaped section

**Fig. 16** Topologies from MTOP using 5,000 B8/n125 elements (volfrac $= 0.2$, $p = 4$, $r_{\min} = 1.0$)



To obtain the same resolution for the cantilever beam, MTOP computation is much more efficient than the element-based approach. MTOP's lower computational cost is mainly attributed to a much lower number of finite elements in a coarse mesh. For example, the number of finite elements of the MTOP coarse mesh in Fig. 10b is 25 times less than that of the fine mesh in Fig. 10a. The efficiency of MTOP over conventional topology optimization is clearer when 3D large-scale problems, in which the finite element analysis cost is a dominant part of the total computational cost, are considered.

### 4.1.4 Multiresolution designs by varying number of density elements per displacement element

We further investigate the influence of the number of density elements per displacement element in the resolution design. Figure 12 shows that the increase of the number of density elements from 4 to 16 improves the resolution of the topology design. Therefore, multiresolution designs can be obtained with the same finite element mesh. However, if the number of density elements is too large, the computational cost for optimization may increase significantly resulting in high total computational cost.

### 4.1.5 Influence of the minimum length scale in resolution design

To investigate the influence of length scale, we vary the minimum length scale from 1.5 to 0.75 for both above-mentioned approaches while keeping the same displacement mesh size of $48 \times 16$. Figure 13 shows that for a length scale larger than the displacement element size ($r_{\min} > 1.0$), the topology obtained from MTOP has better resolution than that from the element-based approach. When the minimum length scale is equal to or smaller than the displacement element size, the element-based approach produces checkerboard solutions. However, for MTOP approach with Q4/n25 element, instabilities were only observed with $r_{\min} < 0.75$.

These results indicate that the MTOP approach can utilize a length scale smaller than the element size, while the element-based approach can only employ a length scale larger than the element size.

### 4.2 Michell truss with a circular support

Michell truss has been used as a verification benchmark for topology optimization (Suzuki and Kikuchi 1991; Sigmund 2000) because the analytical solution is available. For example, a single load transferring to a circular support was investigated by Sigmund (2000), as shown in Fig. 14a. The theoretical optimal solution consisting of orthogonal curve system is shown in Fig. 14b. We investigate this example using the MTOP approach with the domain discretization of $180 \times 120$ Q4/n25 elements. The obtained optimal topology shown in Fig. 14c is very close to the theoretical solution provided by Sigmund (2000).

## 5 Three-dimensional numerical examples

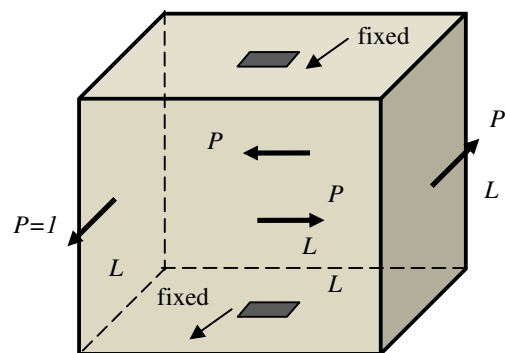This section illustrates the application of our MTOP approach to 3D examples including a cross-shaped section,
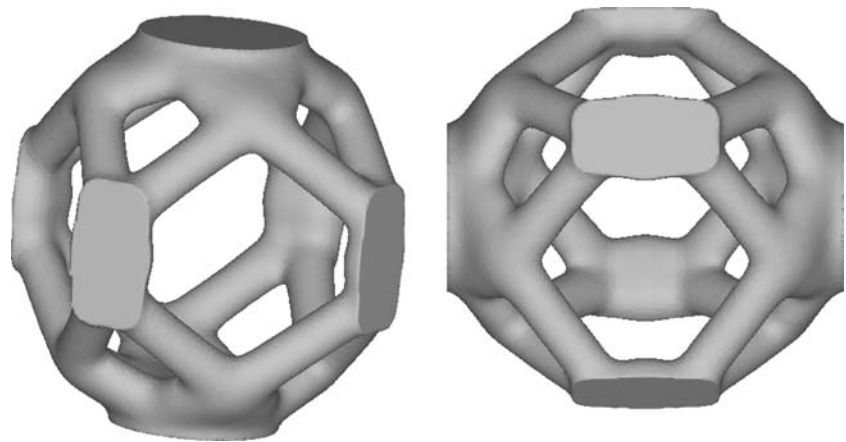


**Fig. 17** Geometry of the cube with lateral loading

**Fig. 18** Topology of the cube
using MTOP 8,000 B8/n125
elements (volfrac = 0.1, $p = 3$,
$r_{\min} = 1.0$)



a cube and a bridge design. The computations of these relatively large problems are performed on a single PC with an Intel® Core(TM)2 Duo 2.00 GHz 32-bit processor, 3 GB RAM of memory, Windows OS, and the code developed in Matlab. Similar to the 2D examples, all the quantities are dimensionless, Young's modulus of 1, and Poison's ratio of 0.3 are employed for computation.

### 5.1 Cross-shaped section

This example is adapted from the study by Borrvall and Petersson (2001) in which a 3D large-scale problem was solved with parallel computing. A cross-shaped domain, which has fixed boundaries on the left and right ends, is subjected to two downward loads applied on its back and front ends as shown in Fig. 15. The dimension of the domain is $L \times 3L \times L$ with $L = 10$. We seek for the optimal design with the volume fraction constraint of 20%. Borrvall and Petersson (2001) discretized the domain into $40 \times 120 \times 120$ B8 elements which results in a total of 320,000 elements and solved this problem with parallel computing. We discretized the domain into $10 \times 30 \times 30$ elements resulting

in a total of only 5,000 B8/n125 elements. Instead of using powerful computing resources, such as parallel computing, with large number of finite elements to solve this problem, we perform the computation in a single PC using MTOP approach with only 5,000 B8/n125 elements and obtain high resolution solution as shown in Fig. 16. Moreover, this optimal topology is similar to the result by Borrvall and Petersson (2001).

### 5.2 Cube with lateral loading

Figure 17 shows a 3D cube which is fixed at the centers of the top and bottom faces. This cube is also subjected to four tangential unit loads at the centers of side faces. The cube domain is discretized into $20 \times 20 \times 20$ B8/n125 elements resulting in a total of 8000 elements. The volume fraction constraint of 10%, minimum length scale $r_{\min} = 1.0$, and penalization $p = 3$ are applied. Figure 18 shows the obtained topology design. The orthogonal curves of the topology indicate that the solution is somewhat similar to the Michell type optimal solution for space truss subjected to torsion loading (Rozvany 1996).

**Fig. 19** Domain for topology
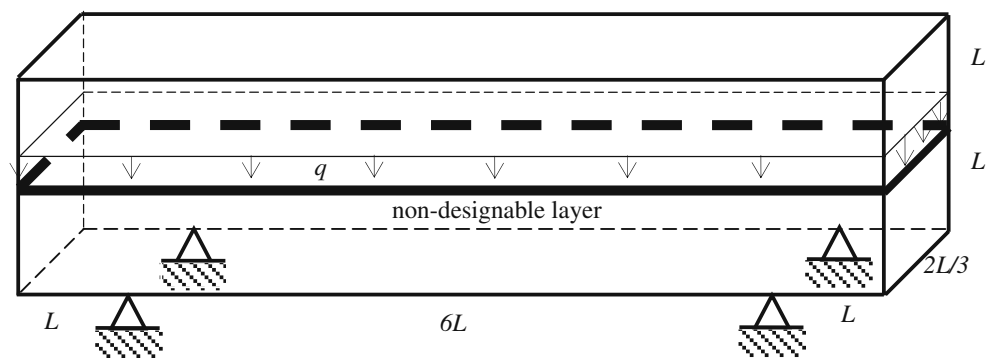optimization of the bridge

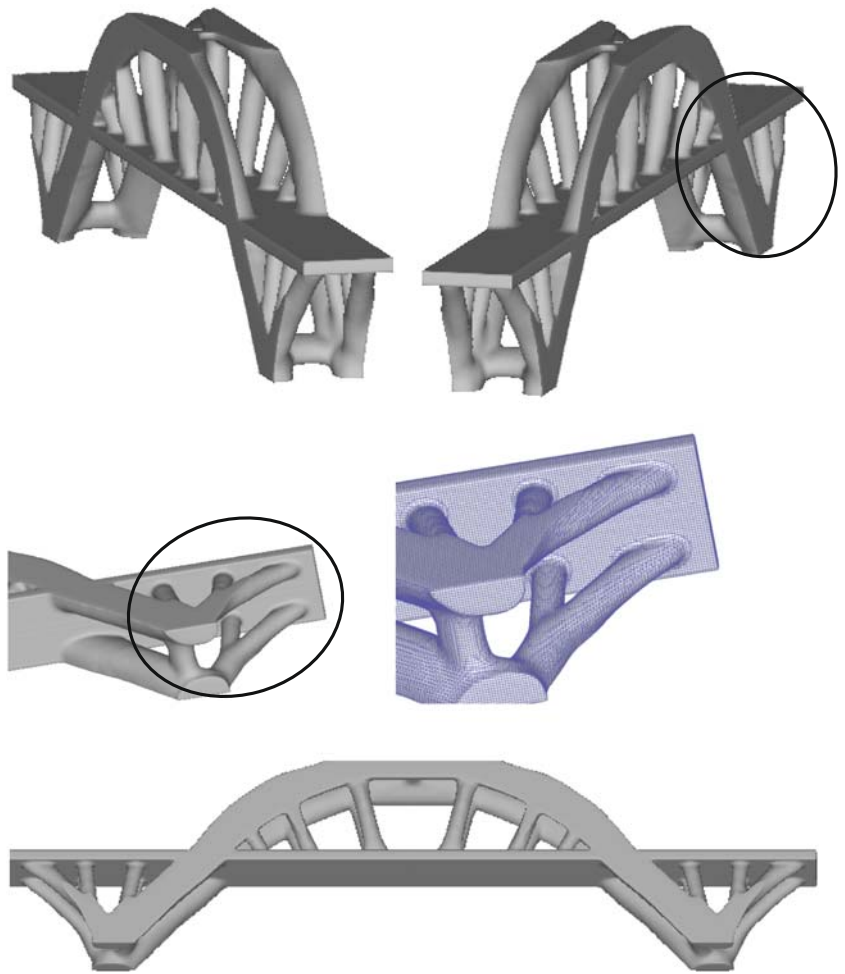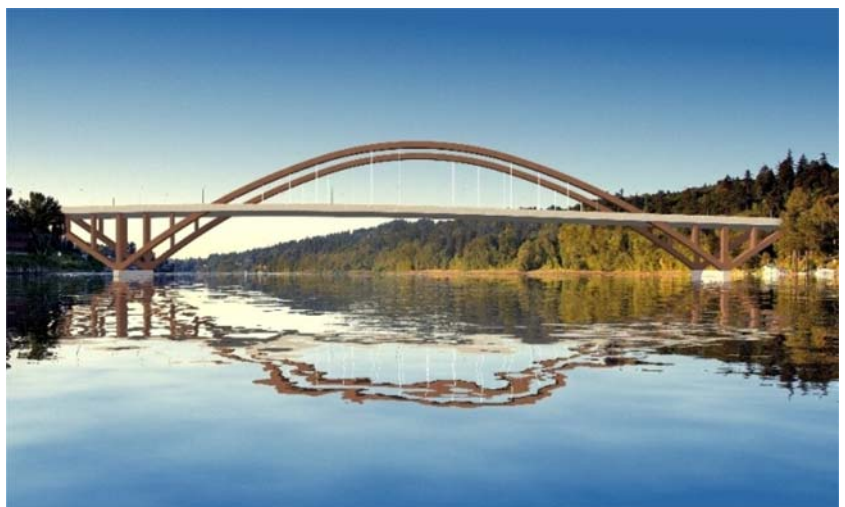**Fig. 20** Optimal topology
of the bridge by MTOP



**Fig. 21** An existing bridge
design (taken from
http://www.sellwoodbridge.org)

## 5.3 Bridge design

Figure 19 presents a 3D bridge topology optimization example with simple supports, cantilevers and a non-designable layer at mid-section. A uniform deterministic unit load $q$ is applied on the top of the non-designable layer of the bridge. The domain is discretized into $10 \times 120 \times 30$ B8/n125 elements. The non-designable layer has a thickness of 1 unit. The volume fraction constraint of 12.0%, the minimum length scale $r_{\min} = 1.0$, and penalization $p = 3$ are employed. The optimal topology as shown in Fig. 20 resembles an existing bridge design shown in Fig. 21.

## 6 Conclusions

In this study, we propose a computational paradigm for multiresolution topology optimization (MTOP). It leads to high resolution designs by employing three different meshes: the displacement mesh, the density mesh, and the design variable mesh. By using design variable and density meshes from coarse to fine, we can obtain multiresolution designs with the same finite element mesh. Furthermore, a projection scheme is introduced to compute element densities from design variables and to control the length scale of the density. Specifically, we employ a coarser displacement mesh and finer density and design variable meshes to obtain high resolution designs with relatively low computational costs. The proposed MTOP approach is demonstrated by various 2D and 3D numerical examples. The MMA is used as the optimizer. Moreover, similar results to the ones presented in this paper were also obtained with the optimality criteria (OC).

This study has shown the advantages of the MTOP approach to obtain high resolution design over conventional topology optimization approaches. Topics for further investigation include the performance of a new projection scheme or smoothening effect. Moreover, the multiresolution topology optimization method may be explored in several fields. For instance, it may have potential advantages in the design of meta-materials and periodic composites with prescribed properties (Paulino et al. 2009), in the solution of multiscale and multiphysics problems (Carbonari et al. 2009), in problems involving other element types such as honeycomb Wachspress elements (Talischi et al. 2009), and in manufacturing constraints (Paulino et al. 2008a, b).

## Nomenclature

| | |
|---|---|
| **d** | vector of design variables |
| $C$ | compliance |
| $V_s$ | prescribed volume |
| $V$ | volume |
| **x** | position of a point in the domain, coordinate vector |
| volfrac | volume fraction |
| $N_i(.)$ | shape function |
| $\mathbf{D}^0$ | constitutive matrix corresponds to the solid material |
| **D** | constitutive matrix |
| **B** | strain-displacement matrix of shape function derivatives |
| **K** | global stiffness matrix |
| $K_e$ | stiffness matrix of displacement element $e$ |
| $\mathbf{K}_e^0$ | stiffness matrix of element $e$ corresponding to the solid material |
| $n$ | number of density elements per displacement element |
| $E$ | Young's modulus |
| $E^0$ | Young's modulus corresponds to solid material |
| $\rho_i$ | density of element $i$ |
| $d_n$ | design variable $n$ |
| $r_{\min}$ | minimum length scale |
| $p$ | penalization parameter |
| $f(.)$ | projection function |
| **u** | global displacement vector |
| **f** | global load vector |
| $A_i$ | area/volume of the density element $i$ in the initial domain |
| $A_i^0$ | area/volume of the density element $i$ in the reference domain |

## References

Almeida SRM, Paulino GH, Silva ECN (2009) A simple and effective inverse projection scheme for void distribution control in topology optimization. Struct Multidisc Optim 39(4):359–371

Amir O, Bendsøe MP, Sigmund O (2009) Approximate reanalysis in topology optimization. Int J Numer Methods Eng 78(12):1474–1491

Bendsøe MP (1989) Optimal shape design as a material distribution problem. Struct Multidisc Optim 1(4):193–202

Bendsøe MP, Kikuchi N (1988) Generating optimal topologies in structural design using homogenization method. Comput Methods Appl Mech Eng 71(2):197–224

Bendsøe MP, Sigmund O (1999) Material interpolation schemes in topology optimization. Arch Appl Mech 69(9–10):635–654

Bendsøe MP, Sigmund O (2003) Topology optimization: theory, methods and applications. Springer, New York

Borrvall T, Petersson J (2001) Large-scale topology optimization in 3D using parallel computing. Comput Methods Appl Mech Eng 190(46–47):6201–6229

Bourdin B (2001) Filters in topology optimization. Int J Numer Methods Eng 50(8):2143–2158

Bruns TE, Tortorelli DA (2001) Topology optimization of non-linear elastic structures and compliant mechanisms. Comput Methods Appl Mech Eng 190(26–27):3443–3459

Carbonari RC, Silva ECN, Paulino GH (2009) Multi-actuated functionally graded piezoelectric micro-tools design: a multiphysics topology optimization approach. Int J Numer Methods Eng 77(3):301–336

Cook RD, Malkus DS, Plesha ME, Witt RJ (2002) Concepts and applications of finite element analysis. Wiley, New York, pp 96–100

de Ruiter MJ, van Keulen F (2004) Topology optimization using a topology description function. Struct Multidisc Optim 26(6):406–416

de Sturler E, Paulino GH, Wang S (2008) Topology optimization with adaptive mesh refinement. In: Proceeding of the 6th international conference on computational of shell and spatial structures, IASS-IACM, 28–31 May 2008. Cornell University, Ithaca, NY, USA

Diaz AR, Sigmund O (1995) Checkerboard patterns in layout optimization. Struct Multidisc Optim 10(1):40–45

Guest JK, Genut LCS (2009) Reducing dimensionality in topology optimization using adaptive design variable fields. Int J Numer Methods Eng. doi:10.1002/nme.2724

Guest JK, Prevost JH, Belytschko T (2004) Achieving minimum length scale in topology optimization using nodal design variables and projection functions. Int J Numer Methods Eng 61(2):238–254

Kim YY, Yoon GH (2000) Multi-resolution multi-scale topology optimization—a new paradigm. Int J Solids Struct 37(39):5529–5559

Matsui K, Terada K (2004) Continuous approximation of material distribution for topology optimization. Int J Numer Methods Eng 59(14):1925–1944

Paulino GH, Le CH (2009) A modified Q4/Q4 element for topology optimization. Struct Multidisc Optim 37(3):255–264

Paulino GH, Almeida SRM, Silva ECN (2008) Pattern repetition in topology optimization of functionally graded material. In: Proceedings of the multiscale, multifunctional and functionally graded materials conference, 22–25 September 2008. Sendai, Japan

Paulino GH, Pereira A, Talischi C, Menezes IFM, Celes W (2008) Embedding of superelements for three-dimensional topology optimization. In: Proceedings of Iberian Latin American congress on computational methods in engineering (CILAMCE)

Paulino GH, Silva ECN, Le CH (2009) Optimal design of periodic functionally graded composites with prescribed properties. Struct Multidisc Optim 38(5):469–489

Pomezanski V, Querin OM, Rozvany GIN (2005) CO-SIMP: extended SIMP algorithm with direct corner contact control. Struct Multidisc Optim 30(2):164–168

Poulsen TA (2002a) Topology optimization in wavelet space. Int J Numer Methods Eng 53(3):567–582

Poulsen TA (2002b) A simple scheme to prevent checkerboard patterns and one-node connected hinges in topology optimization. Struct Multidisc Optim 24(5):396–399

Rahmatalla SF, Swan CC (2004) A Q4/Q4 continuum structural topology optimization implementation. Struct Multidisc Optim 27(1–2):130–135

Rozvany GIN (1996) Some shortcomings in Michell's truss theory. Struct Multidisc Optim 12(4):244–250

Rozvany GIN (2001) Aims, scope, methods, history and unified terminology of computer-aided topology optimization in structural mechanics. Struct Multidisc Optim 21(2):90–108

Rozvany GIN, Zhou M, Birker T (1992) Generalized shape optimization without homogenization. Struct Multidisc Optim 4(3–4):250–252

Sigmund O (2000) Topology optimization: a tool for the tailoring of structures and materials. Philos Trans Math Phys Eng Sci 358(1765):211–227

Sigmund O (2001) A 99 line topology optimization code written in Matlab. Struct Multidisc Optim 21(2):120–127

Sigmund O, Peterson J (1998) Numerical instabilities in topology optimization: a survey on procedures dealing with checkerboards, mesh-dependencies and local minima. Struct Multidisc Optim 16(1):68–75

Stainko R (2006) An adaptive multilevel approach to the minimal compliance problem in topology optimization. Commun Numer Methods Eng 22(2):109–118

Suzuki K, Kikuchi N (1991) A homogenization method for shape and topology optimization. Comput Methods Appl Mech Eng 93(3):291–318

Svanberg K (1987) The method of moving asymptotes—a new method for structural optimization. Int J Numer Methods Eng 24:359–373

Talischi C, Paulino GH, Le CH (2009) Honeycomb Wachspress finite elements for structural topology optimization. Struct Multidisc Optim 37(6):569–583

Wang S, Sturler E, Paulino GH (2007) Large-scale topology optimization using preconditioned Krylov subspace methods with recycling. Int J Numer Methods Eng 69(12):2441–2468